A Neuromechanical Model-Based Strategy to Estimate the Operator's Payload in Industrial Lifting Tasks

Emanuele Feola, Mohamed Irfan Mohamed Refai, Davide Costanzi, Massimo Sartori, *Member, IEEE*, and Andrea Calanca

***Abstract*— One of the main technological barriers hindering the development of active industrial exoskeleton is today represented by the lack of suitable payload estimation algorithms characterized by high accuracy and low calibration time. The knowledge of the payload enables exoskeletons to dynamically provide the required assistance to the user. This work proposes a payload estimation methodology based on personalized Electromyography-driven musculoskeletal models (pEMS) combined with a payload estimation method we called "delta torque" that allows the decoupling of payload dynamical properties from human dynamical properties. The contribution of this work lies in the conceptualization of such methodology and its validation considering human operators during industrial lifting tasks. With respect to existing solutions often based on machine learning, our methodology requires smaller training datasets and can better generalize across different payloads and tasks. The proposed payload estimation methodology has been validated on lifting tasks with 0kg, 5kg, 10kg and 15kg, resulting in an average MAE of about 1.4 Kg. Even if 5kg and 10Kg lifting tasks were out of the training set, the MAE related to these tasks are 1.6 kg and 1.1 kg, respectively, demonstrating the generalizing property of the proposed methodology. To the best of the authors' knowledge, this is the first time that an EMG-driven model-based approach is proposed for human payload estimation.**

***Index Terms*— Payload estimation, electromyography, EMG-based control, industrial exoskeletons, upper-limb exoskeletons, trunk exoskeletons, EMG-driven musculoskeletal modeling.**

Manuscript received 10 August 2023; revised 11 November 2023; accepted 16 November 2023. Date of publication 20 November 2023; date of current version 30 November 2023. This work was supported in part by the European Research Council (ERC) under the European Union's Horizon 2020 Research and Innovation Program, as part of the ERC Starting Grant INTERACT under Grant 803035; and in part by the Socio-Physical Interaction Skills for Cooperative Human Robot Systems in Agile Production (SOPHIA) Project under Grant 871237. *(Corresponding authors: Emanuele Feola; Mohamed Irfan Mohamed Refai.)*

This work involved human subjects or animals in its research. Approval of all ethical and experimental procedures and protocols was granted by the Natural Sciences and Engineering Sciences Ethics Committee of the University of Twente under Reference No. 2022.168.

Emanuele Feola, Davide Costanzi, and Andrea Calanca are with the Department of Computer Science, University of Verona, 37134 Verona, Italy (e-mail: emanuele.feola@univr.it).

Mohamed Irfan Mohamed Refai and Massimo Sartori are with the Neuromechanical Modeling and Engineering Laboratory, Department of Biomechanical Engineering, University of Twente, 7522 NB Enschede, The Netherlands (e-mail: m.i.mohamedrefai@utwente.nl).

Digital Object Identifier 10.1109/TNSRE.2023.3334993

I. Introduction

REGULARLY lifting heavy loads is considered one of the main factors contributing to work-related musculoskeletal disorders [1]. The weight being lifted and the frequency of lifting are associated with the development of chronic low back pain (LBP), due to high mechanical loads resulting in high lumbar joint moments and compression forces [2], [3].

Robotic exoskeletons have the potential to protect musculoskeletal tissues from injury and to reduce the occurrence of chronic musculoskeletal disorders. Industrial exoskeletons are designed with the aim of supporting workers in load-lifting and load-carrying tasks, as well as during quasi static overhead tasks [4].

Industrial exoskeletons can be categorized as either passive, active or semi-active [4], [5]. Passive devices are not powered and rely on elastic components only, while active devices are powered using electric or pneumatic actuators [6], [7], [8]. If passive exoskeletons are characterized by simplicity of design, high wearability and lightweight form factors, active exoskeletons can provide a more versatile physical assistance by modulating the assistive torque. Combining passive and active elements, semi-active exoskeletons [9] can preserve lightweight form factors, while providing highly adaptive solutions. Unfortunately, only a few semi-active or active market-ready devices can be found and they seem to be still under development [7], [8], [10], [11], [12], [13].

One of the main challenges related to the development of such active exoskeletons is providing the appropriate assistive forces when needed [14].

Existing control strategies provide assistance based on the operator's kinematics [15], [16], gravity compensation algorithms [14], [17], [18], [19] but without considering any external payload, proportional myoelectric control [14], [17], [20], or a combination of them [14], [17]. Most of these control strategies are based on manual parameter selection, which usually are payload-dependent and subject-dependent. This involves the operator manually setting the assistance level with a user interface any time the payload and/or the task changes [10], [11], [12], [13]. Surprisingly, although assistive forces should be delivered exactly to compensate for payload-induced forces, none of existing control strategies are based on knowledge or estimation of payload properties,

TABLE I
SUMMARY OF PAYLOAD ESTIMATION/CLASSIFICATION STUDIES. EXISTING PAYLOAD ESTIMATION SOLUTIONS ARE MODEL-BASED AND USE DIRECT FORCE MEASUREMENTS (FORCE PLATES, FORCE SHOES, FORCE/TORQUE SENSORS) AND DO NOT REQUIRE A TRAINING DATASET. INSTEAD, OUR SOLUTION USES AN INDIRECT FORCE MEASUREMENT BASED ON EMG SENSORS

Ref.	Payload Est./Classif.	Input Measurements	EMG Location	Training Payload Conditions	Testing Payload Conditions
[21]	Classification	EMG, Kinematics	Arm	2, 4, 6, 8 kg	same as training
[22]	Classification	EMG	Low back	0, 4.5, 10.8 kg	same as training
[23]	Classification	EMG	Arm	1, 3, 7 kg	same as training
[24]	Classification	EMG, Kinematics	Low back	no payload, symmetric, asymmetric	same as training
[25]	Classification	Kinematics		5, 10, 15 kg	same as training
[26]	Estimation	Force, Kinematics			
[27]	Estimation	Force			
This work	Estimation	EMG, Kinematics	Low back	0, 15 kg	0, 5, 10, 15 kg

such as mass and inertia matrix. This paper exactly addresses this challenge: estimating payload properties to adaptively compensate for payload-induced gravity and inertial forces. A main issue is that the payload is usually not directly attached to the exoskeleton: it is lifted by the operator who is in turn supported by the exoskeleton. Such human inter mediation prevents distinguishing payload-induced forces from human forces. Measuring interaction forces between the human and the exoskeleton does not solve the problem since without knowledge or assumption on human internal forces the identification of payload properties represents a mathematically undetermined problem. Thus, the estimation of human internal forces due to muscular activations becomes of critical importance.

Several studies investigated payload classification through surface electromyography (sEMG) signals [21], [22], [23], [24]. A feasibility study described in [21] considers two armbands with 8 sEMG channels each and an Inertial Measurement Unit. Payload classification during a bicep curling task (2, 4, 6 and 8kg) is proposed using an Artificial Neural Network (ANN). Another study using sEMG and IMU is described in [24]. Authors propose a supervised machine learning classifier to distinguish different payload configurations during gait. Considering a limited sample size, Support Vector Machine is used in [23] to classify 1kg, 3kg and 7kg payloads during an arm flexion task using sEMG. Another study [22] investigated real-time payload classification (0, 4.5, 10.8kg) using multi-nomial logistic regression trained with sEMG during lifting tasks before the time of full payload support by the participant. Other approaches are able to classificate the payload mass without using sEMG. In [25] authors propose a deep-learning network to perform payload classification (5, 10, 15 kg) based on IMU kinematic data only. In [26] authors propose a payload estimation method using IMUs in combination with force plates or sensorized shoes. In [27] authors consider the special case of exoskeletons that directly interact with the payload: force/torque sensors are installed at the payload-exoskeleton interfaces and the payload mass is then easily estimated. Unfortunately, this solution is not adequate for most of industrial exoskeletons where the exoskeleton is not directly attached to the payload and the interaction is mediated by the human.

Table I summarizes the described approaches, which can be categorized as "payload classification" and "payload estimation" approaches. A main difference is that payload classification approaches are limited to the weight instances appearing in the training dataset. This implies that a large training dataset is necessary in the case of several payloads. It can be observed from Table I that all existing payload estimation approaches are not based on sEMG. They use direct force measurements, e.g. force plates, sensorized shoes or force/torque sensors at the robot-payload interfaces, which make the estimation much simpler. Unfortunately, such sensors are not usually available in industrial settings because of costs or feasibility issues.

One of the main issues of estimating human internal forces is the highly non-linear relationship between the measured sEMG and the exerted muscular force [28], [29]. EMG-driven musculoskeletal models inherently account for this non-linearity [30] and represents an alternative to machine learning for estimating muscular forces [29], [30], [31], [32]. Their use in real-time applications have been demonstrated in [32], [33], and [34].

For the first time this work proposes a methodology to estimate payload using an EMG-driven model. The approach is based on the combination of personalized EMG-driven musculoskeletal (pEMS) models and an estimation method we called "delta torque" ($\Delta\tau$) that allows decoupling payload dynamical properties from human dynamical properties. The "delta torque" method is a key building block of our methodology as it does not require the human rigid-body model expressed in closed-form, which is not available in state-of-the-art musculoskeletal modeling tools. As highlighted in Table I, our approach is the only existing EMG-based solution falling in the payload estimation category, and thus able to deal with payload instances not included in the training set. In this study, payload estimation is demonstrated considering sEMG recorded on the back muscles, which poses harder challenges compared to the upper arm muscles considered in other studies [21], [23]. These challenges are due to the complexity of the dynamics between back muscle activations and payload motion. Similarly to existing literature, the payload is regarded as a point mass and the considered lifting tasks are symmetric.

TABLE II
GLOSSARY

Symbol	Definition
m_P	payload mass
$\bar{q}(t)$	joint coordinates that define a specific kinematic task
$\bar{\tau}(t)$	joint torques due to muscle activity necessary to perform $\bar{q}(t)$
$\bar{\tau}(t)^{NP}$	joint torques due to muscle activity necessary to perform $\bar{q}(t)$ in absence of payload (i.e., No Payload)
$\Delta\bar{\tau}(t) = \bar{\tau}(t) - \bar{\tau}(t)^{NP}$	torques difference between loaded and unloaded conditions of the same kinematic task $\bar{q}(t)$
m_P^{pEMS}	approximation of m_P using a pEMS model
m_P^{ID}	approximation of m_P using inverse dynamics with knowledge of the payload mass beforehand. For comparison purposes only.
$\bar{\tau}(t)^{pEMS}$	approximation of $\bar{\tau}(t)$ using a pEMS model
$\Delta\bar{\tau}(t)^{pEMS}$	approximation of $\Delta\bar{\tau}$ using a pEMS model

The paper is organized as follows. Section II outlines the proposed payload mass estimation methodology, which is divided into three distinct steps. Section III describes the performed experimental trials and how the data have been collected and processed. Section IV describes the achieved results. Section V discusses the study results, limitations and future works. Conclusions are reported in Section VI.

II. Proposed Methodology

Let us consider the following equations for a human seen as a multi-body dynamical system

$$\boldsymbol{B(q)\ddot{q} + C(q,\dot{q})\dot{q} + g(q) = \tau - J_R^T(q)F_R - J_L^T(q)F_L} \tag{1}$$

where $\boldsymbol{q} \in \mathbb{R}^n$ represents the generalized coordinates, $\boldsymbol{B(q)} \in \mathbb{R}^{n\times n}$ is the human inertia matrix, $\boldsymbol{C(q,\dot{q})} \in \mathbb{R}^{n\times n}$ is the apparent forces matrix, $\boldsymbol{g(q)} \in \mathbb{R}^n$ is the vector of gravity torques, $\boldsymbol{\tau} \in \mathbb{R}^n$ represents the generalized torques due to human muscles, $\boldsymbol{F_R} \in \mathbb{R}^6$ and $\boldsymbol{F_L} \in \mathbb{R}^6$ represent the Cartesian forces and torques applied at the end-effector of the right and left arms (due to the payload), $\boldsymbol{J_R(q)} \in \mathbb{R}^{6\times n}$ and $\boldsymbol{J_L(q)} \in \mathbb{R}^{6\times n}$ represent the right hand and left hand Jacobians. Since we only considers symmetric lifting tasks we assume that external forces are perfectly balanced between the right and left sides, i.e. $\boldsymbol{F_R = F_L}$. Hence, equation (1) can be simplified to

$$\boldsymbol{B(q)\ddot{q} + C(q,\dot{q})\dot{q} + g(q) = \tau - J^T(q)F_{ext}} \tag{2}$$

where we have the same Jacobian for both upper arms, i.e. $\boldsymbol{J(q) = J_R(q) = J_L(q)}$ and $\boldsymbol{F_{ext} = F_R + F_L}$.

The proposed payload mass estimation approach involves the following steps: Step 1:

Step 1: Estimating joint torques $\boldsymbol{\tau}$ due to muscle activity using state-of-the-art pEMS models;

Step 2: Using the $\Delta\tau$ approach to estimate the external force $\boldsymbol{F_{ext}}$, which is based on the difference in torque between loaded and unloaded conditions of the same kinematic task;

Step 3: Using estimated external forces $\hat{\boldsymbol{F}}_{\boldsymbol{ext}}$ to compute the payload properties

The main advantage of steps 2 and 3 is that to estimate the payload mass we do not need to explicitly compute the matrices $\boldsymbol{B(q)}$, $\boldsymbol{C(q,\dot{q})}$ and $\boldsymbol{g(q)}$ appearing in equation (1). In particular, if we consider a human task characterized by the coordinates $\bar{\boldsymbol{q}}(\boldsymbol{t})$ such that

$$\boldsymbol{B(\bar{q})\ddot{\bar{q}} + C(\bar{q},\dot{\bar{q}})\dot{\bar{q}} + g(\bar{q}) = \bar{\tau} - J^T(\bar{q})F_{ext}}, \tag{3}$$

and we define $\bar{\boldsymbol{\tau}}^{\boldsymbol{NP}}$ as the joint torque corresponding to the same task, i.e. characterized by the same coordinates $\bar{\boldsymbol{q}}(\boldsymbol{t})$, and hypothetically carried out without any payload, such that

$$\boldsymbol{B(\bar{q})\ddot{\bar{q}} + C(\bar{q},\dot{\bar{q}})\dot{\bar{q}} + g(\bar{q}) = \bar{\tau}^{NP}}, \tag{4}$$

then, we easily have

$$\boldsymbol{\Delta\bar{\tau} = \bar{\tau} - \bar{\tau}^{NP} = J^T(\bar{q})F_{ext}} \tag{5}$$

This reveals that by using an estimate of joint torque $\bar{\boldsymbol{\tau}}$ from step 1 and by using inverse dynamics (ID) solvers to compute $\bar{\boldsymbol{\tau}}^{\boldsymbol{NP}}$ it is possible to compute $\Delta\bar{\boldsymbol{\tau}}$ which is directly related to external forces. Then, payload inertial properties can be easily inferred from estimated external forces, as described below. We highlight that describing the payload as external torques and not as within the system is the fundamental point making our approach practically viable. Otherwise, if the payload effects were included in matrices $\boldsymbol{B(q)}$ and $\boldsymbol{C(q,\dot{q})}$ the estimation process would need explicit knowledge of those matrices and would lead to higher complexity, see for instance the load identification approaches proposed in [35] and [36].

Finally, the last step of the proposed approach considers the following relation between external forces $\boldsymbol{F_{ext}}$ and payload mass

$$\boldsymbol{F_{ext} = m_P(a(t) + g)} = \begin{pmatrix} a_x(t)m_P \\ m_P(g + a_y(t)) \\ a_z(t)m_P \end{pmatrix} \tag{6}$$

where m_P represents the payload mass, $\boldsymbol{a} = [a_x, a_y, a_z]^T$ represents the acceleration of the payload and $\boldsymbol{g} = [0, g, 0]^T$ is the gravity acceleration vector. Here we assume that the payload is held near its barycenter and that it is not rotating during motion, which are reasonable assumptions for a wide spectrum of industrial tasks. However, the approach can be extended to payload rotation, to asymmetric tasks and identification of the inertia matrix.

Considering equation (5) the payload mass m_P can be related to the delta torque using the following expression:

$$\Delta\bar{\tau}_i(t) = m_P\boldsymbol{J}_i(\boldsymbol{q})^T \begin{pmatrix} a_x(t) \\ a_y(t) + g \\ a_z(t) \end{pmatrix} \tag{7}$$

where $\Delta\bar{\tau}_i$ is the delta torque element referring to the i-th human joint and $\boldsymbol{J}_i(\boldsymbol{q})$ is the i-th column of the Jacobian matrix, mapping the velocity of the joint i to the end-effector

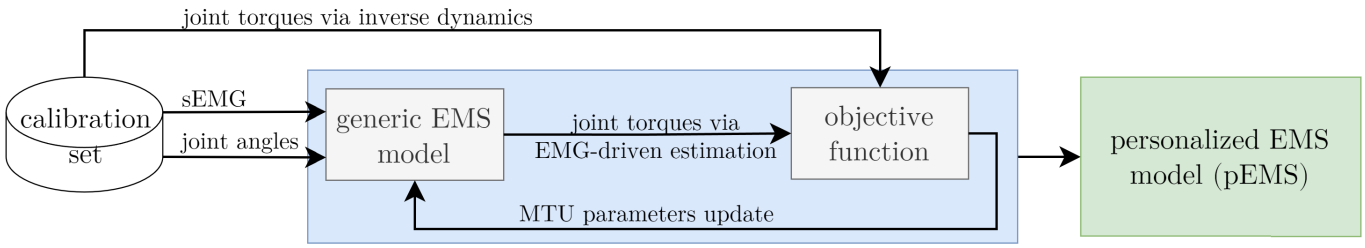

Fig. 1. Calibration pipeline: the blue block represents the calibration process, its inputs are the joint angles, the EMG linear envelopes and the torques computed via inverse dynamics. The output of the calibration process is a calibrated person-specific pEMS model, where MTU parameters are optimized.

velocity. Since we assume the task kinematics is recorded, everything is known except the payload mass m_P and a standard linear regression method can be used to estimate it.

One of the advantages of the proposed approach lies in its versatility: it can be applied to any human joint i by measuring related muscular activations and by selecting different columns of the Jacobian matrix $\boldsymbol{J}(\boldsymbol{q})$. If sEMG are available from several muscles related to different human joints, then a more robust mass estimation can be performed by combining information from multiple joints. This can be done by considering more instances of equation (7) within the same linear regressor. An example is given in section II-C.

A. Step 1: Estimation of Joint Torques Using a pEMS Model

Joint torque estimation is performed using a pEMS model that requires sEMG and joint angles. The pEMS model is built using OpenSim [37], which relies on the multi-body simulator Simbody, and the Calibrated EMG-informed Neuromusculoskeletal (CEINMS) toolbox [29], [38]. The estimation includes three sub-steps.

1) Musculoskeletal Model Design and Scaling: The Lifting Full-Body (LFB) model [39] is used. The LFB model is scaled to the anthropometric measures of the participants using 3D marker data collected during static trials where the participants stood still without movement. As a result of this process, a person-specific skeletal model is produced. In addition to a complete skeletal structure, the LFB model consists of 238 Hill-type muscle-tendon units (MTU) including muscles on the back and on the abdomen. The model was designed for lifting movements with the net trunk motion distributed across six intervertebral joints (S1 until T12) using coupling constraints.

2) Calibration of MTU Parameters: The calibration procedure is required to extract person-specific MTU parameters, which include the tendon slack length, the pennation angle of the muscle fibre at its optimal length, the optimal fibre length at maximum activation, the maximum isometric muscle force, the normalised maximum contraction velocity of the fibre. Calibration is performed once per participant using the CEINMS toolbox, which optimizes the MTU parameters to minimize an objective function based on the error between the joint torque computed using inverse dynamics and EMG-driven estimation. In our case, the calibration set includes the two lifting tasks with 0 kg and 15 kg described in Section III-A. The calibration set comprises only the first half of the tasks. The calibration pipeline is represented in Figure 1.

3) Joint Torque Estimation: The scaled and calibrated pEMS model is used to estimate torque $\bar{\tau}_i^{pEMS}$ at any joint i given the related muscle activity measured using sEMG. In particular, the pEMS model is used to compute forward dynamics (FD) occurring from the onset of muscle activation to the development of muscle forces and joint torque. In our study, the process is driven by muscle activations measured on the lumbar muscles and the output is $\bar{\tau}_{L5S1}^{pEMS}$, i.e. the torque related to the L5S1 flexion-extension human joint.

B. Step 2: Delta Torque Estimation

Once the torque $\bar{\tau}_i^{pEMS}$ is estimated at any joint of interest, the inverse dynamics of the pEMS model is used to compute the human joint torques $\bar{\tau}_i^{NP}$ in unloaded configurations, i.e. as if the payload was not there. Such a hypothetical condition is considered to compute the delta torque as defined in equation (5)

$$\begin{aligned}\boldsymbol{\Delta\bar{\tau}}(t)^{pEMS} &= \begin{bmatrix}\Delta\bar{\tau}_1(t)^{pEMS}\\ \Delta\bar{\tau}_2(t)^{pEMS}\\ \vdots\\ \Delta\bar{\tau}_n(t)^{pEMS}\end{bmatrix}\\ &= \begin{bmatrix}\bar{\tau}_1(t)^{pEMS}-\bar{\tau}_1(t)^{NP}\\ \bar{\tau}_2(t)^{pEMS}-\bar{\tau}_2(t)^{NP}\\ \vdots\\ \bar{\tau}_n(t)^{pEMS}-\bar{\tau}_n(t)^{NP}\end{bmatrix}\end{aligned} \tag{8}$$

where $\Delta\bar{\tau}_i$ is the i-th component of $\Delta\bar{\boldsymbol{\tau}}$ in equation (5) related to the joint i. The quantity $\bar{\tau}_i$ is estimated using a pEMS model and leading to $\bar{\tau}_i^{pEMS}$, as explained in the previous section. The bar symbol in equation (8) just indicates that $\boldsymbol{\Delta\bar{\tau}}$ refers to the specific task whose generalized coordinates are $\bar{\boldsymbol{q}}$.

Finally, in order to compute equation (7) one can use the OpenSim's API to retrieve the Jacobian column $\boldsymbol{J}_i$. Even if the generality of the approach allows estimating the payload properties starting from sEMG measures related to any human joint, we demonstrate the approach considering the L5S1 joint. In this case one needs to consider the specific Jacobian column related to the L5S1 joint which maps the L5S1 joint velocity to the end-effector Cartesian velocity. When the sEMG information is available on multiple muscles related to multiple joints, then multiple columns of the Jacobian can be used to perform a more robust mass estimation. For instance,

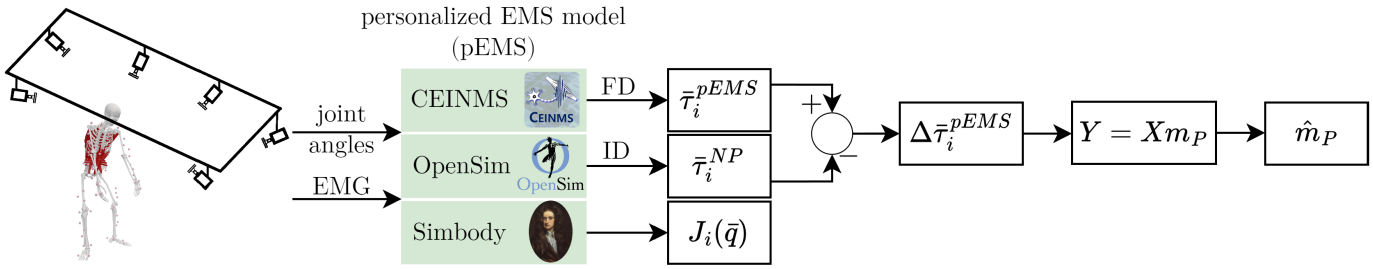

Fig. 2. Delta torque and payload mass estimation pipeline: the calibrated personalized model (pEMS) uses joint angles and EMG data to estimate $\bar{\tau}_i^{pEMS}$, computed using Forward Dynamics. $_1\bar{\tau}_i^{pEMS}$ is computed as the difference between the output of the pEMS model $\bar{\tau}_i^{pEMS}$ and the torque of the same task assumed without external forces, i.e. $\bar{\tau}_i^{NP}$, computed using Inverse Dynamics. Then, the inertial properties of the load are estimated using a least square approach.

if the sEMG information is available on both the elbow and L5S1 joints, the two Jacobian columns can be used.

C. Step 3: Payload Mass Estimation

In this step equation (7) needs to be specialised for this specific case study. Since in our case the sEMG information is available on the muscles related to the L5S1 joint, equation (7) becomes

$$\boldsymbol{\Delta\bar{\tau}}(t)_{L5S1}^{pEMS} = m_P \boldsymbol{J}_{L5S1}(\boldsymbol{q})^T(\boldsymbol{a}(t) + \boldsymbol{g}) \tag{9}$$

where $\boldsymbol{J}_{L5S1}(\boldsymbol{q})^T = \left(\frac{\partial x}{\partial L5S1} \; \frac{\partial y}{\partial L5S1} \; \frac{\partial z}{\partial L5S1}\right)$ represents the first three elements of the column of the Jacobian associated with the L5S1 joint. If we consider the time series of $\boldsymbol{\Delta\bar{\tau}}_{L5S1}^{pEMS}$, this leads to a regression model in the form

$$\boldsymbol{Y} = \boldsymbol{X}m_P$$

where, m_P is the parameter we want to estimate, and $\boldsymbol{Y}$, $\boldsymbol{X}$ are defined as follows:

$$\boldsymbol{Y} = \begin{bmatrix} \Delta\tau_{L5S1}^{pEMS}(\boldsymbol{q}_1) \\ \vdots \\ \Delta\tau_{L5S1}^{pEMS}(\boldsymbol{q}_n) \end{bmatrix}, \quad \boldsymbol{X} = \begin{bmatrix} J_{L5S1}(\boldsymbol{q}_1)(\boldsymbol{a}_1 + \boldsymbol{g}) \\ \vdots \\ J_{L5S1}(\boldsymbol{q}_n)(\boldsymbol{a}_n + \boldsymbol{g}) \end{bmatrix}.$$

The regression model can be solved using the standard least square solution:

$$\hat{m}_P = (\boldsymbol{X}^T\boldsymbol{X})^{-1}\boldsymbol{X}^T\boldsymbol{Y} \tag{10}$$

In the case where sEMG information is available on both the elbow and L5S1 joints, then $\boldsymbol{Y}$ and $\boldsymbol{X}$ can be defined as follows:

$$\boldsymbol{Y} = \begin{bmatrix} \Delta\tau_{L5S1}^{pEMS}(\boldsymbol{q}_1) \\ \Delta\tau_{elbow}^{pEMS}(\boldsymbol{q}_1) \\ \vdots \\ \Delta\tau_{L5S1}^{pEMS}(\boldsymbol{q}_n) \\ \Delta\tau_{elbow}^{pEMS}(\boldsymbol{q}_n) \end{bmatrix} \boldsymbol{X} = \begin{bmatrix} J_{L5S1}(\boldsymbol{q}_1)(\boldsymbol{a}_1 + \boldsymbol{g}) \\ J_{elbow}(\boldsymbol{q}_1)(\boldsymbol{a}_1 + \boldsymbol{g}) \\ \vdots \\ J_{L5S1}(\boldsymbol{q}_n)(\boldsymbol{a}_n + \boldsymbol{g}) \\ J_{elbow}(\boldsymbol{q}_n)(\boldsymbol{a}_n + \boldsymbol{g}) \end{bmatrix}$$

with $\boldsymbol{q}_1 = \boldsymbol{q}(t_1)$ and $\boldsymbol{a}_1 = \boldsymbol{a}(t_1)$. The mass estimated by the least squares solution, denoted as $\hat{m}_P$, is hereon referred to as m_P^{pEMS}.

An overall graphical representation of all estimation steps is proposed in Figure 2.

III. Experimental Trials

A. Experimental Setup

Experimental procedures were approved by the Natural Sciences and Engineering Sciences Ethics committee of the University of Twente (reference number: 2022.168) and all participants gave written informed consent. Nine healthy male participants (average body mass: 67 ± 8 kg; height: 171 ± 8 cm; and age: 28 ± 3 years old) were asked to pick up a box (40 × 30x22 cm) positioned on the ground in front of them, to execute a squat movement and put the box down on the ground. Once the squat task was over and the box was released on the ground, the participants returned to the initial standing position. The squat task is represented in Figure 3. The participants were instructed not to rotate the box while in motion. The participants completed 5 repetitions per weight condition (0, 5, 10 and 15 kg) resulting in the execution of 4 different trials and a total of 20 repetitions. The participants rested for about 1 minute between each trial. During lifting tasks with 0kg, participants lifted a box of negligible weight (about 100 grams), allowing them to perform the task making the same movement as the tasks with a weighted box. We selected a maximum weight of 15kg to prevent participants from experiencing musculoskeletal fatigue with weights higher than 15kg. This would have led to longer experimental trials, providing participants with sufficient time for rest and recovery. Before the actual trial experiments, both an MVC (Maximum Voluntary Contraction) trial and a static trial were recorded. During the MVC trial the participants were instructed to bend their trunk forward and then attempt to return to an upright position while an external force was manually applied to their shoulders. The purpose of this force is to maximally activate the lower back muscles. During the static trial the participant was asked to stay still for about 30 seconds.

B. Data Collection and Processing

A total of 69 markers were placed both on the participant (61) and on the weighted box (8), and their 3D trajectories were recorded at 128 Hz using a twelve-camera motion capture system (Qualisys Medical AB, Sweden). A total of 6 bipolar sEMG sensors were placed bilaterally following SENIAM (Surface ElectroMyoGraphy for the Non-Invasive Assessment of Muscles) [40] guidelines on the following back muscles:

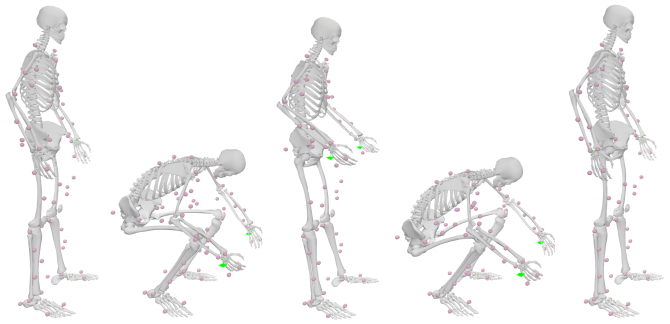

Fig. 3. Squat task: starting from an upright posture, squatting down to pick up the box, lifting the box until upright posture, standing still while holding the box, squatting down to release the box, returning to initial position. Once the sequence is over the participant is back to the starting point.

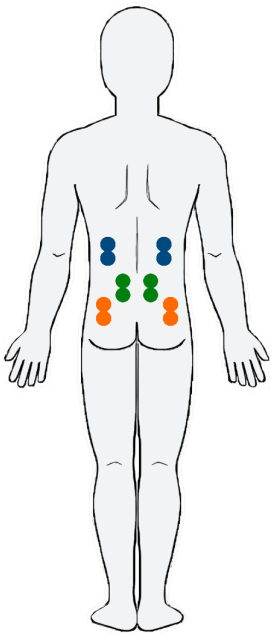

Fig. 4. sEMG sensors are placed bilaterally on the participant's back, targeting the following muscles: Longissimus Thoracis located at 4 cm lateral to T10 (blue sensor), Longissimus Lumborum located at 3 cm lateral to L1 (green sensor), and Iliocostalis Lumborum located at 6 cm lateral to L2 (orange sensor).

Iliocostalis Lumborum, Longissimus Lumborum, Longissimus Thoracis. Figure 4 shows the location of sEMG sensors on the back of a participant. EMG signals were recorded at 2048 Hz using Delsys Bagnoli system (Delsys, Boston, MA). Marker trajectories were low-pass filtered with a second-order zero-phase Butterworth filter (6 Hz). Raw sEMG were bandpass filtered (25-250 Hz), full-wave rectified and low-pass filtered (6 Hz) to obtain EMG linear envelopes. EMG linear envelopes were then normalized using the recorded MVC trials data.

C. Data Analysis

Out of the 9 recorded participants, 7 were analyzed while the remaining 2 were excluded due to problems with sEMG sensor data recording. The recorded marker trajectories are used to perform inverse kinematics analysis allowing the computation of joint angles $\bar{\boldsymbol{q}}(t)$ for each of the lifting tasks.

TABLE III
QUANTIFICATION OF ESTIMATION ERRORS PER WEIGHT CLASS CONSIDERING m_P^{pEMS} PERFORMED BY ALL PARTICIPANTS

	RMSE (kg)	MAE (kg)	$e_{\%}$
Squat 5 kg	1.9	1.6	32 %
Squat 10 kg	1.2	1.1	11 %
Squat 15 kg	1.8	1.5	10 %

The inverse kinematics analysis is performed using OpenSim's Inverse Kinematics Tool. The computed $\bar{\boldsymbol{q}}(t)$ and the recorded sEMG are used to estimate the joint torque $\bar{\tau}_{L5S1}^{pEMS}$ as described in Section II-A and to compute $\Delta\bar{\tau}_{L5S1}^{pEMS}$ as described in Section II-B. The least-square approach described in Section II-C is then used to compute a unique value m_P^{pEMS} for each lifting time window (LTW), i.e. the set of time instants during which the payload is being lifted by the participant. The time instants when the payload is being lifted and released on the ground are assumed known. Since each lifting trial consists of 5 repetitions, 5 different estimated mass values per trial are calculated. Considering all the participants and all the trials, the mean LTW length is 4.5 $\pm$1 seconds. The LTW length is not constant among participants since each one of them held the box for an arbitrary amount of time.

IV. EXPERIMENTAL RESULTS

Figures 5 and 6 show the distribution of the estimated payload mass m_P^{pEMS} for the lifting tasks with 5, 10, 15 kg payloads using blue boxplots. Figures 5 and 6 refers to intra and inter participant data, respectively. Intra-participant analysis evaluates payload estimation results for each participant independently, while inter-participant analysis aggregates payload estimation results from all participants. $RMSE$ (Root Mean Squared Error), MAE (Mean Absolute Error) and R^2 are computed considering the difference between the real and estimated mass values for all the performed tasks and are reported in Figure 5, Figure 6 and Table III. Table III provides an overview of the mass estimation results grouped by payloads showing estimation errors per weight class. In addition to $RMSE$ and MAE, the relative estimation error $e_{\%}$ related to each weight class is also reported. It is computed as $100 * \frac{MAE}{m_P}$. For analysis purposes we reported in Figures 5 and 6 additional gray boxplots which exclude intrinsic noise in sEMG acquisition, modeling and calibration errors. An overview of the different sources of errors possibly affecting the estimation process is reported in Table IV, where "violation of assumptions on the task" regards the modelling assumptions reported in Section V, i.e. left/right symmetry and payload non-rotation, while "computation errors" regards numerical errors in the Jacobian and Inverse Dynamics computation. In Section V, a detailed explanation will be provided on how to isolate individual sources of error from one another.

Finally, we analyzed the baseline noise of sEMG signals in all the performed experiments. We collected the first and last few seconds of each sEMG signal (all 6 recorded channels) when the participants are at rest, i.e. they are standing still and not lifting the box. We computed the variance of these signals

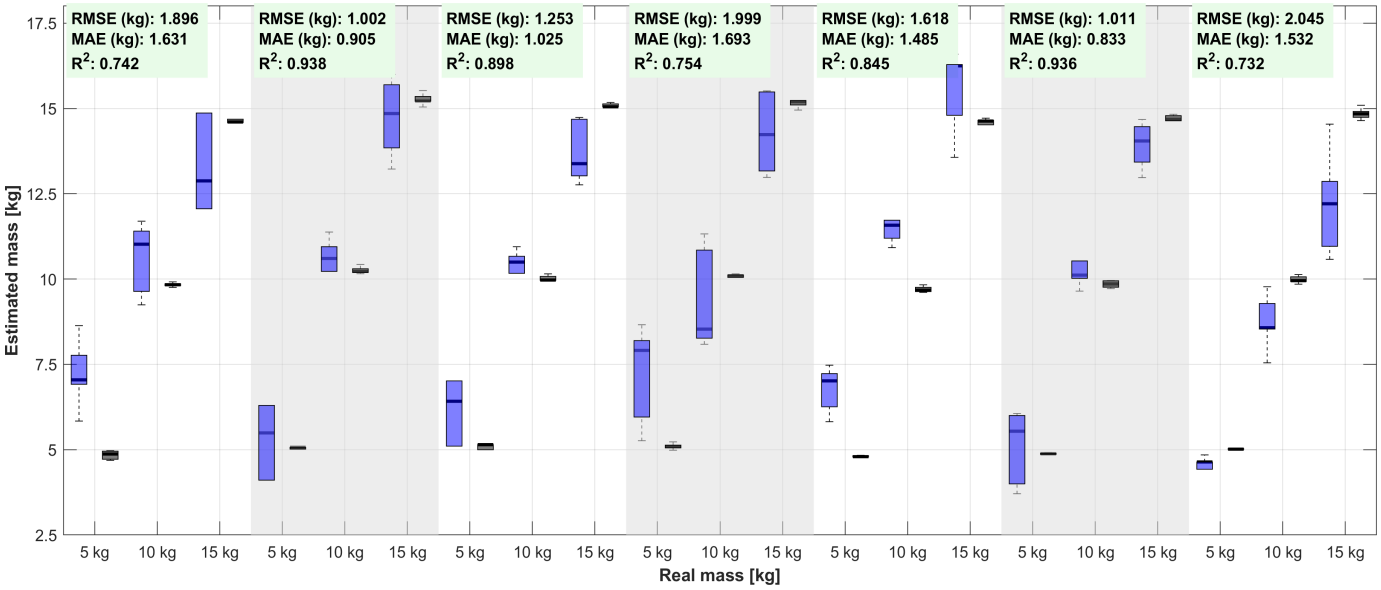

Fig. 5. Analysis of intra-participant results: evaluation of the estimated mass m_P^{pEMS} for each participant. For error analysis purposes, the results of each one of the participants are represented by two boxplots for each squat lifting task with 5, 10 and 15 kg payloads. The blue boxplots represent the mass estimation results m_P^{pEMS}, while the gray boxplots represent the mass estimation results m_P^{ID} that are computed excluding the sources of errors described in Table IV. For each participant, *RMSE*, *MAE*, R^2 are computed considering m_P^{pEMS} of all the tasks performed by that particular participant.

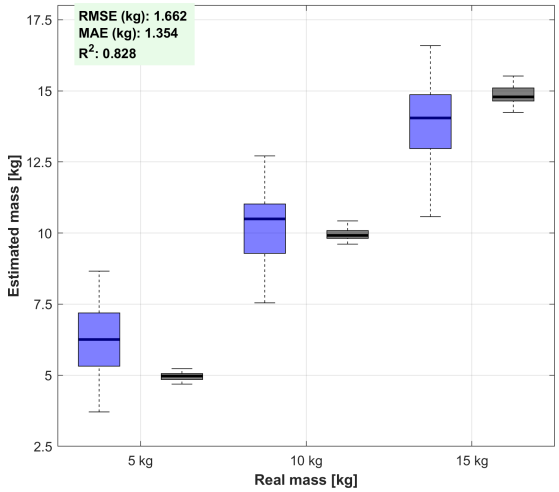

Fig. 6. Analysis of inter-participant results: evaluation of the estimated mass m_P^{pEMS} for each task considering m_P^{pEMS} performed by all participants. The blue boxplots represent the mass estimation results m_P^{pEMS}, while the gray boxplots represent the mass estimation results m_P^{ID} that are computed excluding certain sources of errors, as reported in Table IV. For each lifting task, *RMSE*, *MAE*, R^2 are computed considering m_P^{pEMS}.

and performed paired t-tests to see if there is any statistically significant difference in the variance of the baseline noise of different tasks. We found no statistically significant difference, since all 6 p-values are larger than 0.05.

V. Discussion

We developed and validated a novel payload estimation methodology based on pEMS models and on the "delta torque" approach. Such methodology is driven by sEMG and joint angle information and is able to estimate payload mass instances that are not present in the pEMS calibration set. Our calibration set only include two lifting tasks with 0 and 15kg payloads while the proposed approach was able to accurately estimate any payload instance including 5 kg and 10 kg.

TABLE IV
Payload Mass Estimation Sources of Error. The Assumptions on the Task Are: Task Symmetry and Payload Non-Rotation

Source of error	m_P^{pEMS} (Blue boxplot)	m_P^{ID} (Gray boxplot)
Violation of assumptions on the task	✓	✓
Computation errors	✓	✓
EMG acquisition	✓	
pEMS modeling and calibration (5 and 10kg)	✓	

Figure 6 and Table III summarize the overall result of this work: the proposed payload estimation methodology has an average MAE of about 1.4 Kg. Even if 5kg and 10Kg lifting tasks were out of the training set, the MAE related to these tasks are 1.6 kg and 1.1 kg, respectively, demonstrating the generalizing property of the proposed methodology. Even if the achieved accuracy seems suitable for the considered application, a comparison with other existing EMG-based approaches is not immediate because estimation and classification results are characterized by different performance indicators: false positive/negative for classification and absolute or relative errors for estimation.

The following paragraph reports an analysis related to the sources of errors that can affect the payload mass estimation. As reported in Table IV, we could separate errors due to EMG acquisition and pEMS modeling from other sources of error.

To achieve this separation, we compute the payload mass by replacing $\bar{\tau}_{L5S1}^{pEMS}$ with $\bar{\tau}_{L5S1}^{ID}$ in equation (8). The quantity $\bar{\tau}_{L5S1}^{ID}$ is computed with OpenSim's Inverse Dynamics Tool assuming knowledge of the payload, and without considering EMG data. Since our goal is to estimate the payload, this assumption is not meaningful in practice, but is useful to distinguish sources of error. The payload mass estimated considering this assumption is called m_P^{ID} and is reported in the gray boxplots of Figures 5 and 6. Since m_P^{ID} does not rely on sEMG, it is not affected by sEMG noise and pEMS modeling errors. The reader can observe the great accuracy of m_P^{ID}, meaning that estimation errors are mainly due to sEMG acquisition and pEMS modeling, and not to computation errors and violation of assumptions on the task. Therefore we can conclude that the estimation process is robust to slight asymmetries.

Another point worthy of discussion is that the results indicate a more accurate estimation of heavier weights compared to lighter ones, as evidenced by a larger relative error associated with lighter weights in Table III. This can be due to the following two reasons. First, the sEMG signals recorded in tasks with heavier payloads are characterized by a higher Signal to Noise Ratio (SNR). This is because while baseline noise is the same among different experiments, the sEMG signal amplitude is higher for tasks carried out with heavier payloads. Second, the CEINMS calibration procedure minimizes the error between estimated and measured joint torques, a metric that tends to be larger for tasks involving heavy payloads. This implicitly gives more importance to tasks with heavier payloads. This aspect will be addressed in our future work by revising the CEINMS calibration procedure. Also, future works will include approaches to improve estimation accuracy and robustness to sEMG noise and to modeling errors, including more advanced mass estimation algorithms to solve for m_P in equation (9). Furthermore, measuring multiple muscular activations, related to multiple joints allows to introduce some level of redundancy and therefore to increase robustness. This may be particularly useful in case of singular configurations or when a joint is close to articular limits.

Estimation latency is usually not considered in existing studies. However, in real-world applications the payload mass needs to be computed as quickly as possible. Even if in our work the payload mass estimation is performed considering the entire LTW, whose length is 4.5 seconds, theoretically, a single estimation could be based on a single sample. However, using more samples is essential to filter noise and artefacts. By performing an inter-subject analysis with reduced LTW size, we indeed recorded a slight loss of estimation accuracy. If the LTW size is set to 2 seconds, then $RMSE = 2.1kg$, $MAE = 1.6kg$ and $R^2 = 0.73$, if the LTW size is set to 1 second $RMSE = 2.3kg$, $MAE = 1.8kg$ and $R^2 = 0.66$. Estimation latency minimization will be addressed in our future work.

Furthermore, asymmetric tasks represent a natural extension of our approach and will be considered in future studies. Finally, our future work will entail implementation and testing of payload-adaptive strategies on a real-world assistive exoskeleton. Since exoskeleton assistive torque alters the wearer's muscular activity, this will be modeled in the multibody dynamic model (1) by adding the exoskeleton dynamics and torque contribution.

The implementation on a real-world exoskeleton will also require the real time computation of pEMS model's direct kinematics, inverse and forward dynamics, and Jacobian matrix, which has been demonstrated to be feasible [32], [33], [34].

A. Study Limitations

One of the limitation of this study lies in the type of performed tasks, since only symmetric tasks have been performed. Asymmetric tasks should also be taken in consideration. During an asymmetric task $\boldsymbol{J_R(q)}$ is different from $\boldsymbol{J_L(q)}$ in equation (1), and likewise, the external forces $\boldsymbol{F_R}$ and $\boldsymbol{F_L}$ are not the same since the forces due to the payload are not evenly distributed between left and right sides. Another limiting factor of our validation regards the missing information about abdominal muscles that could have degraded the calibration of the pEMS model and the joint torque estimation. Indeed, we did not measure muscle activity on the abdominal muscles including the Rectus Abdominus, Internal Obliques, External Obliques, which are used to drive the trunk pEMS model [30]. Although these muscles do not have shown significant variations during lifting [30], [41], their absence influences the accuracy in estimating the joint moments at the lower back. As a consequence, measuring abdominal activations may lead to improve our estimation results.

Another limitation is represented by the lifting detection strategy, since the time instants when the payload is being lifted and released on the ground are assumed known. Such assumption can be addressed in real-life scenarios by developing a muscle activity onset detection algorithm. Furthermore, the sample population in this study was limited to male participants, which is another limitation. Additionally, the human-exoskeleton interaction is not yet modeled in the proposed methodology.

VI. Conclusion

For the first time this paper proposes an EMG-driven model-based approach for human payload estimation. The proposed methodology includes the exploitation of pEMS models within a so-called "delta torque" approach.

The proposed methodology has been validated on lifting tasks with 0kg, 5kg, 10kg and 15kg, resulting in an average MAE of about 1.4 Kg. Even if 5kg and 10Kg lifting tasks were out of the training set, the MAE related to these tasks are 1.6 kg and 1.1 kg, respectively, demonstrating its generalizing property. Differently from other works, the proposed methodology is able to estimate weight instances not included in the calibration set, thus reducing the time needed for calibration. Also, the method is not based on recognizing task-specific motion patterns and - once calibrated on the subject - can easily generalize over a wide repertoire of activities. Finally, the proposed solution does not rely on external expensive sensors (e.g. force plates) and the input data may be acquired from wearable sensors fostering applicability of the approach to real-world scenarios.

REFERENCES

[1] B. R. D. Costa and E. R. Vieira, "Risk factors for work-related musculoskeletal disorders: A systematic review of recent longitudinal studies," *Amer. J. Ind. Med.*, vol. 53, pp. 285–323, Mar. 2010.

[2] P. Coenen et al., "The effect of lifting during work on low back pain: A health impact assessment based on a meta-analysis," *Occupat. Environ. Med.*, vol. 71, no. 12, pp. 871–877, Dec. 2014.

[3] P. Coenen, I. Kingma, C. R. L. Boot, P. M. Bongers, and J. H. van Dieën, "Cumulative mechanical low-back load at work is a determinant of low-back pain," *Occupat. Environ. Med.*, vol. 71, no. 5, pp. 332–337, May 2014.

[4] T. Moeller, J. Krell-Roesch, A. Woll, and T. Stein, "Effects of upper-limb exoskeletons designed for use in the working environment—A literature review," *Frontiers Robot. AI*, vol. 9, Apr. 2022, Art. no. 858893.

[5] H. Lee, W. Kim, J. Han, and C. Han, "The technical trend of the exoskeleton robot system for human power assistance," *Int. J. Precis. Eng. Manuf.*, vol. 13, no. 8, pp. 1491–1497, Aug. 2012.

[6] M. P. de Looze, T. Bosch, F. Krause, K. S. Stadler, and L. W. O'Sullivan, "Exoskeletons for industrial application and their potential effects on physical work load," *Ergonomics*, vol. 59, no. 5, pp. 671–681, May 2016.

[7] A. Voilqué, J. Masood, J. C. Fauroux, L. Sabourin, and O. Guezet, "Industrial exoskeleton technology: Classification, structural analysis, and structural complexity indicator," in *Proc. Wearable Robot. Assoc. Conf. (WearRAcon)*, Mar. 2019, pp. 13–20.

[8] S. Toxiri et al., "Back-support exoskeletons for occupational use: An overview of technological advances and trends," *IISE Trans. Occupat. Ergonom. Hum. Factors*, vol. 7, nos. 3–4, pp. 237–249, Oct. 2019.

[9] S. Crea et al., "Occupational exoskeletons: A roadmap toward large-scale adoption. Methodology and challenges of bringing exoskeletons to workplaces," *Wearable Technol.*, vol. 2, Sep. 2021, Art. no. e11.

[10] (2023). *Agade Exoskeletons*. [Online]. Available: https://agade-exoskeletons.com/en/home-english-2/

[11] (2023). *Cray X*. [Online]. Available: https://germanbionic.com/en/solutions/exoskeletons/crayx/

[12] T. Walter, N. Stutzig, and T. Siebert, "Active exoskeleton reduces erector spinae muscle activity during lifting," *Frontiers Bioeng. Biotechnol.*, vol. 11, Apr. 2023, Art. no. 1143926.

[13] (2023). *Exo Active*. [Online]. Available: https://www.festool.com/blog/news/exoactive

[14] S. Toxiri et al., "Rationale, implementation and evaluation of assistive strategies for an active back-support exoskeleton," *Frontiers Robot. AI*, vol. 5, p. 53, May 2018.

[15] Z. Luo and Y. Yu, "Wearable stooping-assist device in reducing risk of low back disorders during stooped work," in *Proc. IEEE Int. Conf. Mechatronics Autom.*, Aug. 2013, pp. 230–236.

[16] B. Chen, L. Grazi, F. Lanotte, N. Vitiello, and S. Crea, "A real-time lift detection strategy for a hip exoskeleton," *Frontiers Neurorobotics*, vol. 12, p. 17, Apr. 2018.

[17] H. Hara and Y. Sankai, "Development of HAL for lumbar support," in *Proc. SCIS ISIS*, 2010, pp. 416–421.

[18] H. K. Ko, S. W. Lee, D. H. Koo, I. Lee, and D. J. Hyun, "Waist-assistive exoskeleton powered by a singular actuation mechanism for prevention of back-injury," *Robot. Auto. Syst.*, vol. 107, pp. 1–9, Sep. 2018.

[19] M. Lazzaroni et al., "Acceleration-based assistive strategy to control a back-support exoskeleton for load handling: Preliminary evaluation," in *Proc. IEEE 16th Int. Conf. Rehabil. Robot. (ICORR)*, Jun. 2019, pp. 625–630.

[20] T. Lenzi, S. M. M. De Rossi, N. Vitiello, and M. C. Carrozza, "Intention-based EMG control for powered exoskeletons," *IEEE Trans. Biomed. Eng.*, vol. 59, no. 8, pp. 2180–2190, Aug. 2012.

[21] R. Oboe, A. Tonin, K. Yu, K. Ohnishi, and A. Turolla, "Weight estimation system using surface EMG armband," in *Proc. IEEE Int. Conf. Ind. Technol. (ICIT)*, Mar. 2017, pp. 688–693.

[22] D. Totah, L. Ojeda, D. D. Johnson, D. Gates, E. M. Provost, and K. Barton, "Low-back electromyography (EMG) data-driven load classification for dynamic lifting tasks," *PLoS ONE*, vol. 13, no. 2, Feb. 2018, Art. no. e0192938.

[23] S. Aziz, M. U. Khan, F. Aamir, and M. A. Javid, "Electromyography (EMG) data-driven load classification using empirical mode decomposition and feature analysis," in *Proc. Int. Conf. Frontiers Inf. Technol. (FIT)*, Dec. 2019, pp. 272–2725.

[24] M. Goršič, B. Dai, and D. Novak, "Load position and weight classification during carrying gait using wearable inertial and electromyographic sensors," *Sensors*, vol. 20, no. 17, p. 4963, Sep. 2020.

[25] M. Pesenti, G. Invernizzi, J. Mazzella, M. Bocciolone, A. Pedrocchi, and M. Gandolla, "IMU-based human activity recognition and payload classification for low-back exoskeletons," *Sci. Rep.*, vol. 13, no. 1, Jan. 2023, Art. no. 1184.

[26] Y. Tirupachuri et al., "Online non-collocated estimation of payload and articular stress for real-time human ergonomy assessment," *IEEE Access*, vol. 9, pp. 123260–123279, 2021.

[27] X. Wang, Q. Song, S. Zhou, J. Tang, K. Chen, and H. Cao, "Multi-connection load compensation and load information calculation for an upper-limb exoskeleton based on a six-axis force/torque sensor," *Int. J. Adv. Robot. Syst.*, vol. 16, no. 4, Jul. 2019, Art. no. 172988141986318.

[28] A. V. Hill, "The maximum work and mechanical efficiency of human muscles, and their most economical speed," *J. Physiol.*, vol. 56, nos. 1–2, pp. 19–41, Feb. 1922.

[29] M. Sartori, M. Reggiani, D. Farina, and D. G. Lloyd, "EMG-driven forward-dynamic estimation of muscle force and joint moment about multiple degrees of freedom in the human lower extremity," *PLoS ONE*, vol. 7, no. 12, Dec. 2012, Art. no. e52618.

[30] A. Moya-Esteban, H. van der Kooij, and M. Sartori, "Robust estimation of lumbar joint forces in symmetric and asymmetric lifting tasks via large-scale electromyography-driven musculoskeletal models," *J. Biomechanics*, vol. 144, Nov. 2022, Art. no. 111307.

[31] D. G. Lloyd and T. F. Besier, "An EMG-driven musculoskeletal model to estimate muscle forces and knee joint moments in vivo," *J. Biomech.*, vol. 36, no. 6, pp. 765–776, Jun. 2003.

[32] M. Sartori, D. G. Lloyd, M. Reggiani, and E. Pagello, "A stiff tendon neuromusculoskeletal model of the knee," in *Proc. IEEE Workshop Adv. Robot. Social Impacts*, Nov. 2009, pp. 132–138.

[33] K. Manal, K. Gravare-Silbernagel, and T. S. Buchanan, "A real-time EMG-driven musculoskeletal model of the ankle," *Multibody Syst. Dyn.*, vol. 28, nos. 1–2, pp. 169–180, Aug. 2012.

[34] M. Sartori, L. Gizzi, D. G. Lloyd, and D. Farina, "A musculoskeletal model of human locomotion driven by a low dimensional set of impulsive excitation primitives," *Frontiers Comput. Neurosci.*, vol. 7, p. 79, Jun. 2013.

[35] C. G. Atkeson, C. H. An, and J. M. Hollerbach, "Estimation of inertial parameters of manipulator loads and links," *Int. J. Robot. Res.*, vol. 5, no. 3, pp. 101–119, Sep. 1986.

[36] J. Swevers, W. Verdonck, B. Naumer, S. Pieters, and E. Biber, "An experimental robot load identification method for industrial application," *Int. J. Robot. Res.*, vol. 21, no. 8, pp. 701–712, Aug. 2002.

[37] S. L. Delp et al., "OpenSim: Open-source software to create and analyze dynamic simulations of movement," *IEEE Trans. Biomed. Eng.*, vol. 54, no. 11, pp. 1940–1950, Nov. 2007.

[38] C. Pizzolato et al., "CEINMS: A toolbox to investigate the influence of different neural control solutions on the prediction of muscle excitation and joint moments during dynamic motor tasks," *J. Biomech.*, vol. 48, no. 14, pp. 3929–3936, Nov. 2015.

[39] E. Beaucage-Gauvreau et al., "Validation of an OpenSim full-body model with detailed lumbar spine for estimating lower lumbar spine loads during symmetric and asymmetric lifting tasks," *Comput. Methods Biomechanics Biomed. Eng.*, vol. 22, no. 5, pp. 451–464, Apr. 2019.

[40] H. J. Hermens, B. Freriks, C. Disselhorst-Klug, and G. Rau, "Development of recommendations for SEMG sensors and sensor placement procedures," *J. Electromyogr. Kinesiol.*, vol. 10, no. 5, pp. 361–374, Oct. 2000.

[41] J. Schnieders, V. V. Harmelen, and S. J. Wagemaker, "The effect of the Laevo FLEX exoskeleton on muscle activity and perceived exertion," Laevo Exoskeletons B.V, EX Rijswijk, The Netherlands, Tech. Rep., Apr. 2023. [Online]. Available: https://static1.squarespace.com/static/5f7d9bb22f1bc82b03f6f1b0/t/642c17304b46474b2bf9a295/1680611123737/2023-04+-+Laevo+FLEX+EMG+measurement+-+white+paper.pdf

Open Access funding provided by 'Università degli Studi di Verona' within the CRUI CARE Agreement